

DNA Translocations through Nanopores under Nanoscale Preconfinement

Kyle Briggs,[†] Gregory Madejski,[‡] Martin Magill,[§] Konstantinos Kastritis,[§] Hendrick W. de Haan,[§] James L. McGrath,[‡] and Vincent Tabard-Cossa^{*,†}

[†]Department of Physics, University of Ottawa, Ottawa, Ontario K1N 6N5, Canada

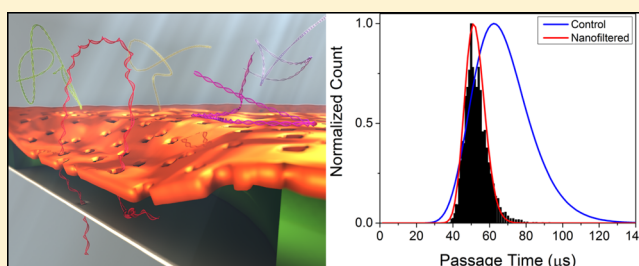
[‡]Department of Biomedical Engineering, University of Rochester, Rochester, New York 14627, United States

[§]Faculty of Science, University of Ontario Institute of Technology, Oshawa, Ontario L1H 7K4, Canada

S Supporting Information

ABSTRACT: To reduce unwanted variation in the passage speed of DNA through solid-state nanopores, we demonstrate nanoscale preconfinement of translocating molecules using an ultrathin nanoporous silicon nitride membrane separated from a single sensing nanopore by a nanoscale cavity. We present comprehensive experimental and simulation results demonstrating that the presence of an integrated nanofilter within nanoscale distances of the sensing pore eliminates the dependence of molecular passage time distributions on pore size, revealing a global minimum in the coefficient of variation of the passage time. These results provide experimental verification that the inter- and intramolecular passage time variation depends on the conformational entropy of each molecule prior to translocation. Furthermore, we show that the observed consistently narrower passage time distributions enables a more reliable DNA length separation independent of pore size and stability. We also demonstrate that the composite nanofilter/nanopore devices can be configured to suppress the frequency of folded translocations, ensuring single-file passage of captured DNA molecules. By greatly increasing the rate at which usable data can be collected, these unique attributes will offer significant practical advantages to many solid-state nanopore-based sensing schemes, including sequencing, genomic mapping, and barcoded target detection.

KEYWORDS: Nanopore, nanotechnology, nanofabrication, DNA, entropy, nanoconfinement



When a single biopolymer such as DNA translocates a nanopore, the dynamics of molecular transport are complex.^{1–5} The speed during passage is thought to be dependent on the fraction and conformation of the molecule outside the pore,⁶ as well as being subject to thermal fluctuations and transient interactions with the pore walls and membrane materials.^{7–9} The net effect is for the molecular motion to be afflicted by a wide distribution of passage speeds, both due to inter- and intramolecular velocity fluctuations.¹ Such a spread in passage times confounds simple translation of time to molecular position, complicating mapping applications, and greatly limits the ability of the nanopore to distinguish charged molecules by size compared to traditional gel-based electrophoresis techniques.

Most experimental efforts aimed at controlling the speed of molecular translocation through a solid-state nanopore have focused on slowing DNA by various means, including interfacing the pore with a gel;^{10,11} by judicious choice of electrolyte, both aqueous¹² and ionic-liquid;¹³ by laser-modulating the surface charge density;¹⁴ by adjustment of the viscosity;¹⁵ or by using different membrane materials.^{16,17} While these methods are able to slow DNA translocations to

varying degrees, they generally do so at the cost of wider passage time distributions.

Few studies have considered the factors that contribute to the wide distributions of passage times. Experimentally, the choice of salt solution has been shown to have a significant effect on the width of passage time distributions,¹² while a pore with diameter matched to the size of DNA limited DNA self-interaction and reduced the variation in passage time.¹⁸ Barcoded molecules have also been used to explore intramolecular variation in passage times, revealing speed up toward the end of the translocation,¹⁹ and it was found that Brownian motion alone is insufficient to explain the observed variations.^{20,21} Simulation work, on the other hand, has demonstrated that polymers are perturbed from equilibrium by the extended electric field gradient during the capture process,²² changing the passage time distribution compared to equilibrium predictions. In addition, molecules which are extended prior to translocation have longer passage times due to increased drag forces.⁶

Received: September 20, 2017

Revised: October 27, 2017

Published: October 31, 2017

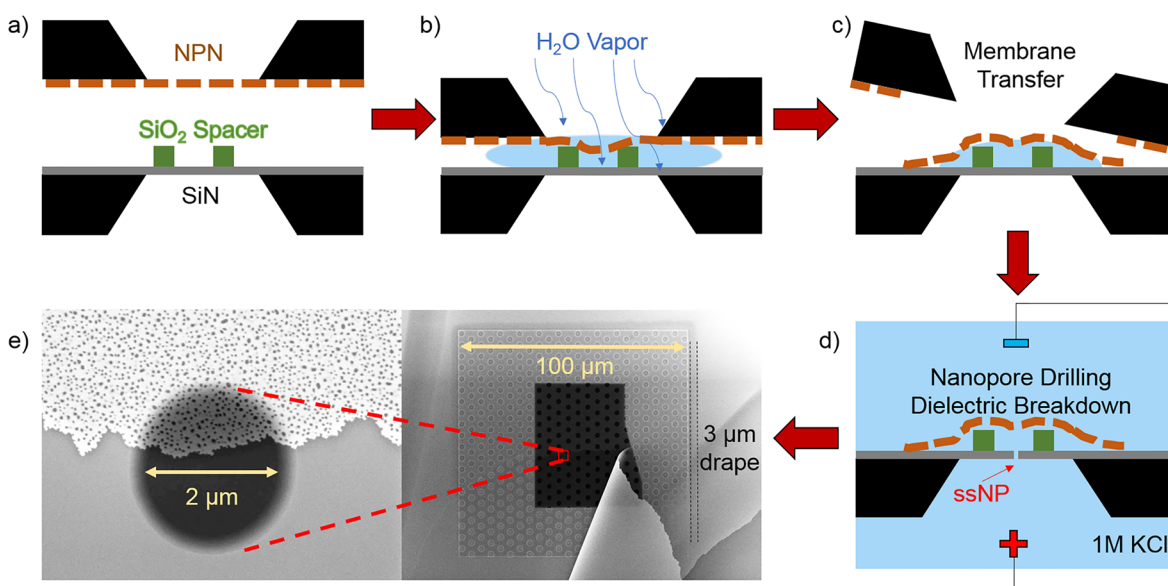


Figure 1. (a) 50 nm NPN membrane is aligned to a 20 nm SiN membrane, patterned with a 200 nm SiO₂ spacer. (b) Condensation of water vapor penetrates the NPN membrane, inundates the nanocavity, and draws the NPN membrane to the SiO₂ spacer. (c) The NPN membrane is torn away from the carrier chip by surface tension and remains attached to the SiO₂ spacer and SiN surface. (d) Nanopore fabrication by a controlled breakdown with the nanofilter already in place. (e) SEM image of a device after step c. A section of NPN membrane is torn away, revealing the SiO₂ spacer underneath. The pore may be formed in any oxide microwell in the darker central region, which corresponds to the free-standing SiN membrane. The device shown in this SEM image has a 2 μm microwell, whereas the devices used in the rest of the paper use 1 μm microwells.

Unfortunately, while the dominant mechanism responsible for high variability in passage time is thought to be the large conformational entropy available to DNA molecules prior to translocation through the nanopore,²³ experimental verification has remained difficult due to the complexity of fabricating devices with sufficiently confining geometries in the vicinity of a nanopore.^{24–27} Recent work, employing the confining geometry of nanopipette-based conical nanopores, has provided evidence that polymer entropy prior to translocation is related to mean passage time but did not consider the standard deviation.²⁸ In this work, we present the first experimental verification that entropy reduction through preconfinement of DNA reduces the passage time variation inherent in nanopore transport processes. Confinement is achieved by taking advantage of the extreme flexibility and permeability of ultrathin (50 nm) nanoporous silicon nitride (NPN) membranes^{29,30} to place them within nanoscale distances of a solid-state nanopore sensor while still allowing fluidic contact in an innovative single-molecule biosensor configuration.

The nanofiltered nanopore device architecture realizes a two-membrane system, comprised of an ultrathin, nanoporous layer of 50 nm thick NPN membrane, separated by a 200 nm gap from a 20 nm thick silicon nitride (SiN) membrane. This essentially creates an architecture comprising two pores in series. NPN is a recently developed highly porous nanomembrane technology with tunable pore sizes (20–80 nm) and porosities (1–40%).²⁹ The gap between the nanofilter and SiN membranes is achieved through the lithographic patterning of a hexagonal grid of 1 μm diameter holes in a 200 nm thick SiO₂ layer deposited on top of SiN. A backside etch then creates a freestanding SiN membrane beneath cylindrical SiO₂ cavities spaced 5 μm apart. The nanofilter is passively held in place directly above these oxide wells, most likely by van der Waals forces. A schematic and electron microscopy images of the device assembly process are shown in Figure 1.

Unless otherwise noted, the nanofilter membranes used in this work had a porosity of 5%, with an average pore diameter of 49 ± 8 nm (mean \pm standard deviation), corresponding to a number density of ~ 25 pores/ μm^2 . With this setup, each 1 μm diameter circular oxide microwell (0.785 μm^2) contains 20 ± 5 pores. Wetting of the space between the membranes is achievable due to the extraordinary high gas permeability of the ultrathin nanofilter membrane.³¹ This device is mounted in a fluidic flow-through cell, exposed to an aqueous salt solution, and a single nanopore is fabricated in the SiN membrane using controlled breakdown (CBD), described elsewhere.^{32,33} The CBD process produces a single nanopore in one of the oxide wells at random.³⁴ Due to the low electrical resistance of ultrathin highly porous NPN, the presence of the nanofilter has negligible effect on CBD and on the electrical characteristics of the resulting single nanopore (referred to hereafter as the sensing pore). Further details of the NPN material properties, pore fabrication process, and nanosensor electrical characterization are presented in Supplementary Section S1.

Simulations were also conducted to better understand the behavior of nanofiltered pores. A standard coarse-grained polymer model was used to model the DNA chains.³⁵ The driving electric field was solved numerically between the nanofilter and the sensing pore, and approximated analytically elsewhere. Only a single pore in the nanofilter was explicitly represented in simulations, placed 150 nm off-axis from the sensing pore, which was located in the center of the microwell. Further details of the simulation setup are provided in Supplementary Section S2.

Double-stranded DNA (dsDNA) molecules of lengths varying from 100 bp to 4000 bp are introduced to the cis (nanofilter) side of the system and are driven through the system by a voltage bias of 200 mV in 3.6 M LiCl pH 8 unless otherwise noted. Because the resistance of the sensing pore dominates that of the nanofilter, the current blockage that is sensed is due entirely to the interaction between dsDNA

molecules and the sensing pore, while the nanofilter remains electrically invisible. Interestingly, the capture rate of nanofiltered devices is comparable to the capture rate of control devices in most cases. Detailed event counts and capture rates are available in [Supplementary Table S1](#) and [Supplementary Section S3](#).

Following Mihovilovic et al.,³⁶ we define type 1 events to be single-file passage of dsDNA, type 21 events to be partially folded events in which the event begins in the folded state. More complex event shapes are indicated by longer strings of integers, which correspond to integer multiples of the single-file dsDNA blockage in the order in which they appear. Events containing levels which do not correspond to an integer multiple of the level 1 blockage are labeled anomalous and are excluded from subsequent analysis. These comprise less than 5% of events overall and are typically attributed to interactions of DNA with the access regions of nanopores,³⁷ or to fitting artifacts.

We first consider the kinetics of passage of molecules which pass the sensing pore in an unfolded type 1 configuration. [Figure 2a–c](#) show schematic representations of possible conformations of dsDNA prior to translocation through the sensing pore. As can be seen in [Figure 2d](#), when $N \lesssim 1300$ bp, there is a single population of passage times for single-file passage which is well-characterized by a log-normal distribution. For $N \gtrsim 1300$ bp ([Figure 2e](#) and [f](#)), a one-sided tail

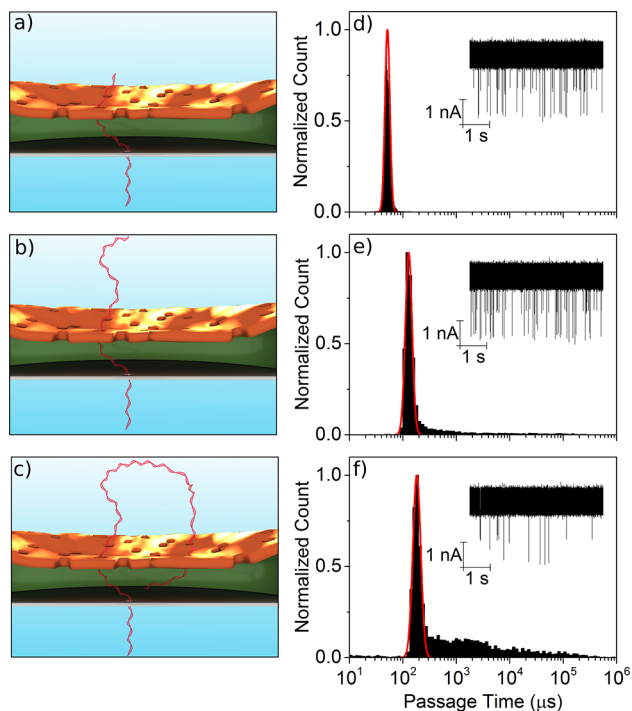


Figure 2. (a, b, c) Schematic representations of 1000, 2000, and 3000 bp dsDNA traversing the nanofiltered pore device, respectively. Vertical distance and DNA length is to scale. (d, e, f) Passage time histograms of unfolded type 1 events for the corresponding lengths of dsDNA. All three histograms are obtained using the same pore, while the pore grew during the course of the experiment (4.3 h), from top to bottom, from 6.7 nm, to 7.3 nm, and finally to 8.0 nm, respectively. Insets: time series of dsDNA translocations (including folded events) for the corresponding histogram. Data recorded at 4.166 MHz sampling rate, digitally filtered with a low-pass Bessel filter at 900 kHz, and down-sampled to 2.5 MHz for plotting.

appears in addition to the log-normal component, comprising events with very long passage times. We attribute the log-normal portion of the passage time distributions to unhindered passage through the two serial membranes. Details of the analysis, along with event counts, are shown in [Supplementary Section S3](#).

[Figure 3](#) shows properties of unhindered dsDNA passage time distributions as a function of the number of base pairs N , representing fits to data extracted from a total of 1.3 million individual DNA translocations through eight nanofiltered pores and seven control pores.

The mean passage time τ for nanofiltered pores is fitted well by a single power law,

$$\tau(N) = \tau_0 N^p \quad (1)$$

which yields an exponent of $p_{\text{exp}} = 1.19 \pm 0.06$, as shown in [Figure 3a](#). This exponent is in reasonable agreement with previous studies on regular solid-state nanopores.^{36,38,39} Error bars define the 95% confidence interval for the fit parameters. Control devices without the nanofilter ([Figure 3b](#)) behave similarly, but with slightly larger spread in mean passage times. Simulations ([Figure 3c](#)) also show power law scaling, though the exponent, $p_{\text{sim}} = 1.61 \pm 0.02$, is larger than in the experimental case. This is consistent with previous work, since simulations typically find scaling exponents which are larger than those extracted from experiments.^{40,41}

The effect of the nanofilter becomes more apparent when considering the standard deviation σ of the passage time ([Figure 3d–f](#)), where the nanofilter usually results in significantly lower standard deviations than the control case. Experimental data with the nanofilter are fitted by a two-power law:

$$\sigma(N) = \sigma_0 \left(\left(\frac{N}{N^*} \right)^q + \left(\frac{N}{N^*} \right)^r \right) \quad (2)$$

The experimental best-fit exponents for this form are $q_{\text{exp}} = 0.5 \pm 0.3$ and $r_{\text{exp}} = 2.0 \pm 0.6$, in reasonable agreement with $q_{\text{sim}} = 0.3 \pm 0.5$ and $r_{\text{sim}} = 2.1 \pm 0.2$ for the simulated data. The standard deviation thus exhibits a crossover between different power laws for small and large N , as discussed below.

As a consequence of the mean and standard deviation passage times scaling behavior, the coefficient of variation σ/τ exhibits nonmonotonic behavior and has a global minimum which can be seen in [Figure 3g](#) and [i](#). The origins of this minimum can be explained by examining the simulation data for the translocation time and standard deviation ([Figure 3c](#) and [f](#)). At short lengths, the standard deviation grows weakly with increasing DNA length. In this limit, the DNA is rod-like, and thus increasing the length of the DNA causes minute variations in the available conformations at the start of translocation. On the other hand, for rod-like polymers, the friction coefficient grows approximately with the length of the rod,⁴² and thus, the translocation time does increase significantly. Hence, a weakly growing standard deviation normalized by an increasing translocation time yields a decreasing coefficient of variation. This rod-like limit breaks down around the Kuhn length, where the variation of initial conformations increasingly influences the distribution of translocation times. Indeed, the standard deviation is seen to increase strongly with increasing length for $N > 300$ bp (slightly above the Kuhn length in simulations). The onset of this additional source of variation causes the increase in standard

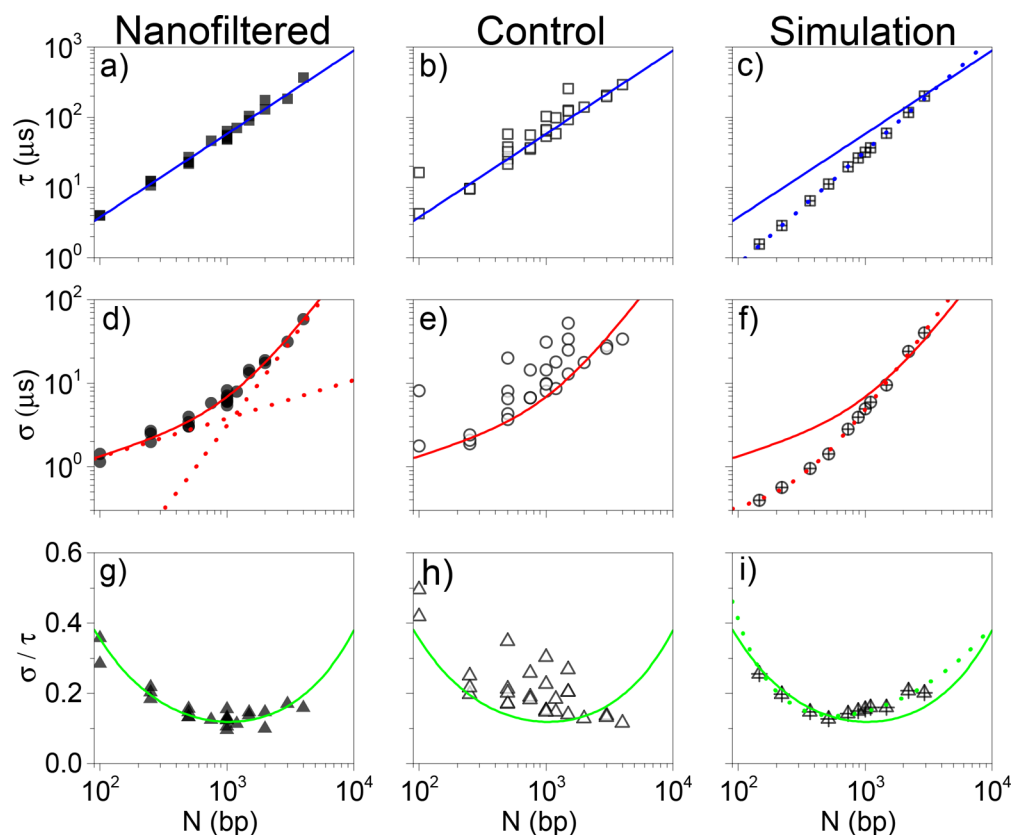


Figure 3. Mean passage times for (a) nanofiltered, (b) control, and (c) simulated nanofiltered pores as a function of DNA length. The solid blue lines are a fit of eq 1 to the data in a, while the dashed line in c is a fit to the simulated data. Standard deviation of passage times for (d) nanofiltered, (e) control, and (f) simulated nanofiltered pores. The solid red lines are a fit of eq 2 to the data in panel d. The dotted lines in d show the two power laws separately, while the dotted line in f shows the two-power fit to the simulated results. Coefficient of variation for (g) nanofiltered, (h) control, and (i) simulated nanofiltered pores. The solid green lines are the quotient of the fits in a and d, while the dotted line in panel i is the quotient of the fits to simulated data.

deviation to outpace that in the mean passage time, thus increasing the coefficient of variation. The combination of these effects is a minimum between these two regimes.

In the controls (Figure 3e), we see that deviations from the fit to nanofiltered pore data are always biased toward larger standard deviations (note the log scale). For a given molecular size, sensing pores equipped with a nanofilter set a lower bound for the standard deviation that is achievable by the sensing pore. To understand this trend, we consider recent simulation work which showed that the gradient in the electric field outside of nanopores can stretch out polymers as they are captured prior to translocation since polymer segments that are closer to the pore experience a larger electrophoretic force than those further away.^{22,43} The distance from the pore at which elongation occurs can be estimated by considering the capture distance at which the electrophoretic force overcomes diffusion, which is proportional to the square of the pore diameter.⁴⁴ The experimental data in Figure 4 are collected for several devices in which the sensing pore diameter was varied between 3 and 14 nm. This translates into a variation of the capture distance over more than an order of magnitude. Hence, in the absence of the nanofilter, the DNA will be consistently elongated for large pores but much less so for small pores. The effects of this are experimentally observed in the control data in Figure 4b: large pores exhibit a smaller variation in the conformation of the dsDNA prior to translocation and thus a smaller standard deviation in the translocation times compared to the more

variable conformations expected for smaller pores. In the presence of the nanofilter, sufficiently long dsDNA must uncoil to thread through the nanofilter and is thus biased to approach the sensing pore in an elongated conformation independent of the sensing pore size. Consequently, the nanofilter reduces the variability in the initial conformation and improves the standard deviation beyond what can be consistently achieved with large sensing pores alone and more importantly removes the dependence of passage time standard deviation on sensing pore size and stability. We demonstrate that this effect can be used to improve the resolution and the reliability of nanopore polymer size spectroscopy, an application which is discussed in Supplementary Section S4.

It is also interesting to note that the normalized mean passage time has a pore size dependence, with smaller control pores actually leading to slower translocation than their nanofiltered counterparts. Since an elongated polymer is expected to have more drag and thus take more time to translocate,⁶ this is counterintuitive. We attribute this observation to additional friction arising from interactions between the coiled polymers that approach small control pore both with itself (coil–coil interactions) and the surrounding membrane (coil–membrane interactions), as depicted in Figure 4d. Because these polymers are not elongated, their conformation renders them more prone to interact with the membrane surrounding the mouth of the pore, potentially leading to temporary weak sticking, whereas elongated

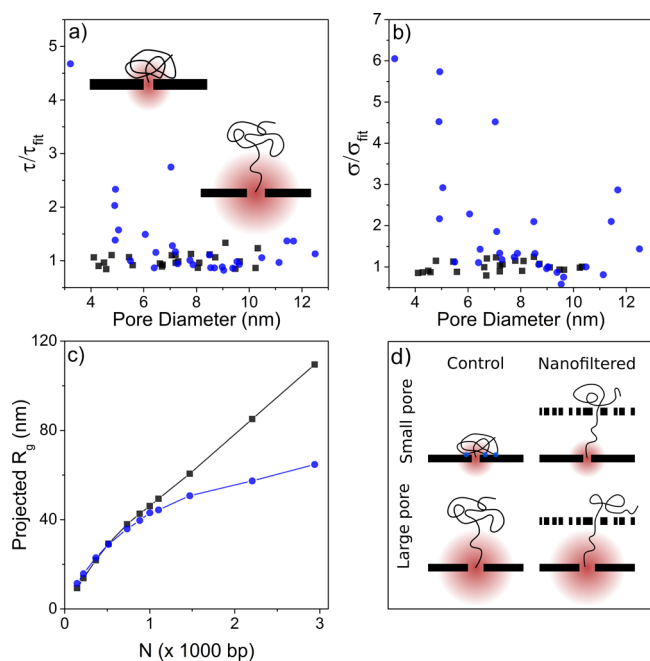


Figure 4. (a) Experimental mean passage times normalized by the fit of eq 1 as a function of sensing pore size for both nanofiltered (black squares) and control pores (blue circles). Inset schematics show the stretching of the polymer as it enters the capture radius of control pores for two different pore sizes. (b) Experimental standard deviation normalized by the fit of eq 2 as a function of sensing pore size. (c) Simulated projection of the radius of gyration on the vector connecting the sensing pore and the center of mass of the DNA at the moment of capture, for molecules initialized with one end in the nanofilter (black squares) versus one end in the sensing pore (blue circles). (d) Schematics illustrating the expected conformations of polymers at the onset of translocation for small and large pores with and without the nanofilter. Red gradients depict the electric profile outside the pore, while blue dots represent the potential interaction sites between the polymer and the membrane outside the pore.

polymers will not be subject to this slowing effect. The proposed mechanisms slowing translocation in the control pores are explored in more detail in [Supplementary Section S5](#).

To further elucidate the origin of the minimum in the coefficient of variation and to confirm that molecules which pass through the nanofilter tend to be more elongated than those that do not, additional simulations were conducted wherein the dsDNA was initialized by equilibrating with one end fixed in the sensing pore (Figure 4c). In this configuration, DNA are much less elongated on average. However, in these simulations where the nanofilter plays little to no role, the crossover in the standard deviation of the passage time and the global minimum in the coefficient of variation are still observed, albeit at slightly shorter chain lengths. The fact that this crossover behavior is also visible as the lower bound in the control experiments for both standard deviation (Figure 3d) and the coefficient of variation (Figure 3g) point to a molecular property of the polymers, namely, the polymer stiffness, being responsible for the presence of the minimum in the coefficient of variation, rather than the presence of the nanofilter. The nanofilter is the mechanism by which the sensing pore can achieve the minimal standard deviation required to actually map the transition. Therefore, fundamental physics of polymer translocations are revealed by the presence of the nanofilter. This crossover behavior has always been present but has until now been indistinguishable from noise.

In principle, prestretching of the polymer is not the only way in which to achieve a reduction in the standard deviation of the passage time. As long as the conformational entropy is reduced, the passage time will be more consistent regardless of the subset of conformation space that is selected. Different confining geometries prior to translocation through the pore can in theory produce similar effects.²³ However, Figure 4a suggests that membrane interactions may play an important role in variability in the translocation process. Prestretching is capable of mitigating membrane interactions while simulta-

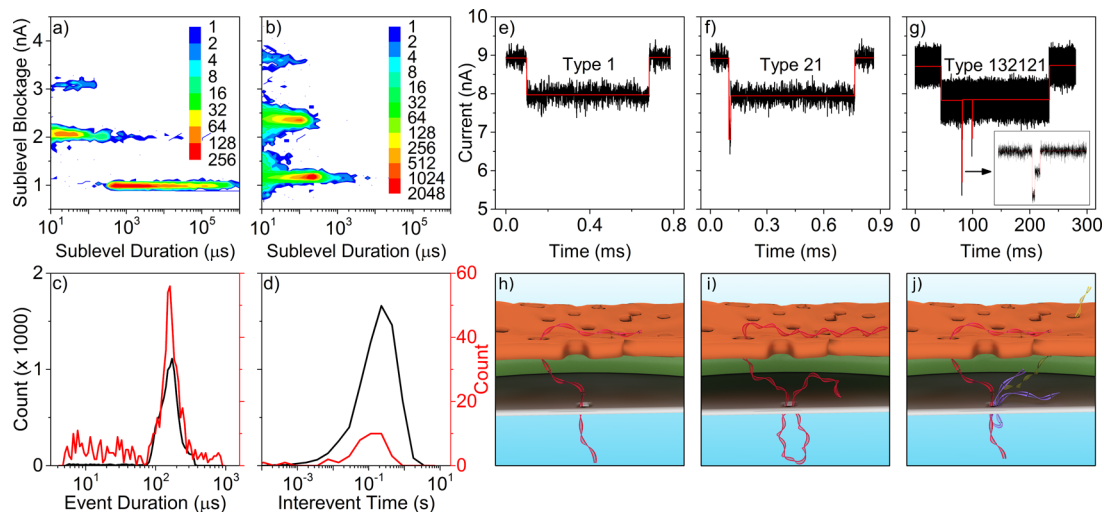


Figure 5. (a) Heat map of sublevels within events, showing blockage depth as a function of sublevel duration for events which fall within the tail of long events for 3000 bp dsDNA in an 8.0 nm nanofiltered pore. (b) For comparison, the sublevel breakdown for a control pore (no nanofilter), showing that the long tail of events is absent. (c, d) Distribution of passage times and interevent times respectively for superimposed events within long single-level events (red) compared to the passage time distribution for unhindered events from the same pore (black). (e–g) Examples of a single-level, unfolded type 1 event, a briefly initially folded type 21 event, and a more complex event, respectively, from among the 3000 bp double-threaded events. (h–j) schematic representations of the molecular conformations giving rise to each of the corresponding event signatures above. Red DNA represents a polymer which is adsorbed to the filter, while other colors translocate freely.

neously reducing conformational entropy, which need not be the case for any confining geometries.

While large control pores can sometimes approach the performance of nanofiltered pores, the results presented in Figures 3 and 4 show that the presence of the nanofilter idealizes the sensing pore, allowing the system to consistently achieve a minimal standard deviation and coefficient of variation. In addition, a remarkable feature of nanofiltered pores is the fact that this minimization happens independent of sensing pore size. In several cases the pore size was observed to grow over the course of a single experiment (Supplementary Table S1), without compromising the improvement to the passage time characteristics. This independence of the sensor on both pore size and pore stability, made possible by the presence of the nanofilter within nanoscale distances of the sensing pore, is a feature of clear importance to many solid-state nanopore-based technologies.

We attribute the long events which appear in Figure 2e and f to translocation which has one end of the dsDNA temporarily adsorbed to the nanofilter during capture of the other end by the sensing pore. Several other plausible explanations for the long events are discussed and ruled out in Supplementary Section S6. To support this picture, we define adsorbed events as events with passage times exceeding four standard deviations above the mean for the log-normal portion of the passage time distribution on a log-scale. Figure 5a shows the sublevel blockage depth as a function of duration for all of the events with long passage times for 3000 bp molecules translocating a nanofiltered pore. It can be compared to the full set of sublevels for a similar control pore (Figure 5b), which does not have the extended tail of long events. While most long events show a single blockage level (Figure 5c and h), blockage states corresponding to occupation of the pore by more than one dsDNA molecule are present in some events. These deeper blockage levels are always very short compared to the unfolded sublevel and for the majority of events appear only at the very start of events (type 21, Figure 5f and i). These latter events correspond to a dsDNA adsorbed on the nanofilter, which is captured in a folded configuration very near an end and then proceeds to occupy the pore in an unfolded conformation for the remainder of its length. However, there is a significant population of complex events which contain levels corresponding to two and three times the single occupation level in the middle of an extended stretch of single occupancy, which cannot generally be explained by interactions of a single molecule with the pore (Figure 5g and j). We attribute these superimposed events to simultaneous translocation of a second, unhindered dsDNA molecule, while the pore is partially occluded by a single DNA molecule adsorbed on the nanofilter. To support this, we note that the passage time distributions for superimposed events are similar to those for regular unhindered events (Figure 5c). The interevent time distributions for superimposed events are also consistent with the unhindered translocations (Figures 5d).

As dsDNA length increases even further, the passage time distribution eventually becomes dominated by long events as all of the molecules thread through multiple pores in the nanofilter and arrive with both ends in the sensing pore in a double-threaded configuration. The sensing pore then exhibits very predictable clogging modes closely matching the expected blockage level for folded dsDNA, which we attribute to simultaneous capture of both ends of the DNA by the sensing pore while it is double-threaded through two pores in the

nanofilter. Additional discussion of clogging by long molecules is presented in Supplementary Section S6.

In addition to augmenting the standard deviation of molecular passage time distributions through a nanopore, the large degree of conformational entropy available to semiflexible polymers also leads to folded translocation, in which a polymer is captured from somewhere along the length of the molecule and translocates in a hairpin conformation. This is particularly problematic for genomic mapping and barcoding schemes in which a DNA molecule is tagged with a marker, either to determine the presence or location of a particular sequence,^{45–47} the presence of a target,²⁰ or to map the velocity profile of translocating molecules.¹⁹ In such applications, folded translocations are generally excluded from data analysis, which can result in having to ignore many translocation events entirely. As a result, ensuring single-file passage of dsDNA through pores of any size is of high technological importance for many diagnostic and genomics applications^{20,45,47,48} that rely on detecting and mapping bound probes. While it is possible to restrict folding by using a nanopore too small to allow it, this is often incompatible with bulky labeling schemes and can be sensitive to pore instability.^{49,50}

We observed complete elimination of dsDNA folding during translocation through the sensing pore in two nanofiltered pore devices, despite the sensing pore being sufficiently large in both cases to allow for folded passage. The first of these pores is discussed in detail in Supplementary Section S7. Both of these devices had in common a low event rate compared to the rest of the nanofiltered devices. Due to the variability of folding behavior between nanofiltered devices, the origin of this effect must lie with the particular details of each individual nanofilter. We hypothesize that the mechanism behind folding suppression is the variation in the local distribution of nanofilter pore positions in the vicinity of the sensing pore. As discussed in Supplementary Section S7, only a small number of nanofilter pores which are very close to the sensing pore are active and have a sufficiently high electric field to capture dsDNA, so the local nanofilter pore distribution can be different between devices. In particular, if a device has two active nanofilter pores which are very close together compared to the extent of the dsDNA, the probability of a dsDNA molecule threading through both nanofilter pores will be high. Because of the electric field gradient between the two membranes, double-threaded polymers will tend to favor capture by one end, and translocation will proceed unfolded due to the resulting elongation.

To test this hypothesis, we performed experiments using a different nanofilter material, which had slightly smaller pores (38 ± 12 nm) but higher porosity ($16 \pm 3\%$), yielding more closely spaced nanofilter pores which would promote double-threading. Due to the smaller nanofilter pores, a higher voltage of 400 mV was required to obtain a sufficiently high event rate to gather statistics.

A dramatic demonstration of the hypothesized physical picture is shown in Figure 6. The device suppressed folding almost completely during the first part of the experiment (Figure 6a and b). Subsequently, the sensing pore clogged and exhibited increased noise centered around a single-occupancy clog for a few minutes. When the clog cleared the sensing pore, with the open pore current baseline returning to its previous value, subsequent events presented folding (Figure 6a and c). The most likely explanation is that one of the two closely spaced nanofilter pores was permanently clogged during the

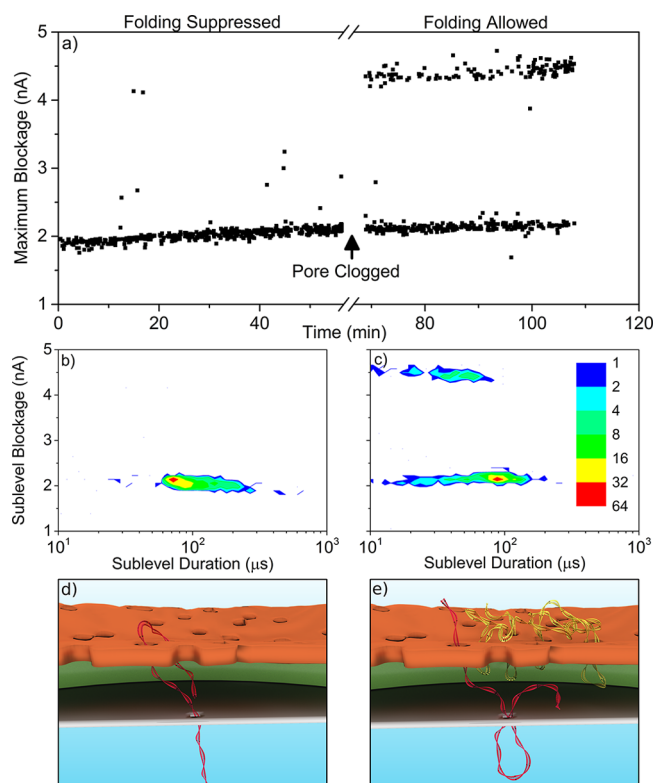


Figure 6. (a) Maximum blockage as a function of experiment time, showing near-complete suppression of folding during the first half of the experiment, followed by allowing folding after a period of prolonged clogging. The single-occupancy blockage level is around 2 nA for this 5.4 nm sensing pore. (b) Heat map of the sublevels for events from the folding-suppressed half of the experiment. (c) Heat map of the sublevels for events from the folding-allowed half of the experiment, following clogging of the sensing pore. (d) Schematic of the hypothesized mechanism of folding suppression consisting of two closely spaced nanofilter pores. (e) Schematic depicting how the folding suppression can be lost when one or more of the active nanofilter pores is clogged.

period in which the sensing pore was clogged, and since the local properties of the nanofilter no longer promoted double-threading, folding was no longer suppressed.

In light of this, we expect that folding suppression can be achieved reliably if the nanofilter parameters can be chosen so as to promote double threading of DNA molecules en route to the sensing pore. As long as the edge-to-edge distance between adjacent active nanofilter pores is smaller than the free solution radius of gyration of the polymer, we expect this probability to be high, while small nanofilter pores will promote unwinding of the dsDNA molecule as it passes into the space between the membranes. Further discussion of folding kinetics can be found in [Supplementary Section S7](#).

One of the reasons preconfinement of molecules through the use of two-membrane systems has proven experimentally challenging is the difficulty inherent in producing two adequately spaced, precisely sized, serial nanopores while having fluidic access to the nanoscale gap between them for the purposes of wetting. The nanofiltered pore device presented herein creates a composite structure which achieves an optimal balance between these requirements while keeping the complexity minimal: the ultrathin, porous nanofilter material allows easy wetting and simple fluidic and electrical access to the intermediate space for the purposes of nanopore

fabrication by CBD, which guarantees the presence of appropriately aligned nanopores without requiring visual confirmation, and eliminates both the requirement for precise nanopore size and the deleterious effects of size instability during sensing.

The combined simulation and experimental results obtained on this nanofiltered pore device demonstrate the strong influence the capture process has on the dynamics of DNA translocation and reveal the presence, previously hidden in the noise, of a minimum in the normalized variance of translocation times that is inherent to semiflexible polymers. The presence of the nanofilter upstream of the nanopore sensor prestretches the polymer, which offers a significant reduction in variation of passage times. This composite structure will enable a broad range of applications and provide enhanced sensing capabilities. It can be leveraged to provide more precise polymer size separation and to suppress folded translocations, thus forcing single-file passage, of critical importance for many life science and health applications, including DNA sizing, barcoded target detection, and genome mapping.

Methods. Nanofilter Assembly. The NPN nanofilter membranes and SiN/oxide microwell substrate chips (SiMPore Inc., West Henrietta, NY) are cleaned with a nitrogen flow, followed by 38 W air plasma for 40 s to make all surfaces hydrophilic. Both the substrate and nanofilter chips are placed into gentle contact using a custom aluminum jig and placed in a -15°C freezer for 2 min to cool below room temperature. The assembly is then exposed to fine mist produced by a vaporizer, which condenses on the cooled surface and fills the cavity between the two membranes. As the liquid evaporates through the nanofilter, surface tension pulls the two membranes into contact, which then remain sealed together once all of the liquid has evaporated. The two chips are then separated mechanically, and the nanofilter is left behind in contact with the substrate chip. To completely seal the nanofilter and to reduce chip capacitance, polydimethylsiloxane (PDMS) is then painted over the entire chip surface, leaving only the free-standing membrane portion exposed. This assembly can be stored until use.

Just before use, the assembly is air plasma cleaned at 38 W for 40 s to make all surfaces hydrophilic. The cleaned assembly is then placed in a sealed container with ambient air (40% humidity), and this container is placed in the -15°C freezer for up to 5 min. The cooling condenses humidity in the microwell, wetting the gap between the two membranes.

Nanopore Fabrication by CBD. Nanopores are fabricated in nanofilter assemblies via CBD, which is described elsewhere.³² Briefly, pores are formed in 1 M KCl pH 10 using a slowly increasing voltage ramp from -10 V to -18 V applied to the nanofilter side of the assembly, with the trans side grounded. Typical fabrication times are between 5 and 10 min. Once fabricated, the salt solution is changed to 3.6 M LiCl pH 8, and depending on the initial pore size, the diameter is adjusted using 3–4 V 4s square voltage pulses until the desired pore in the range of 6–15 nm is achieved. Depending on the IV and noise characteristics, pores are sometimes aged before use.⁷

Data Acquisition and Analysis. NoLimits dsDNA molecules (Life Technologies Inc.) in the range of 100–4000 bp are premixed to the desired concentration (between 3 and 76 nM) and injected into the vicinity of the pore using a custom PEEK flow cell.

Data are acquired in MATLAB R2013a (32-bit) using the Chimera VC100 current amplifier with 200 mV applied unless

otherwise noted, sampled at 4.166 MHz, with a hardware two-pole low-pass Bessel filter at 1 MHz cutoff frequency. Data are postfiltered for analysis at 900 kHz using a digital low-pass Bessel filter and analyzed to extract passage times and sublevel structure using both the adept2state module of MOSAIC^{51,52} (<https://pages.nist.gov/mosaic/>) for 100 bp molecules which do not fold, and a custom implementation of the CUSUM+ algorithm^{52,53} for the rest of the events (<https://github.com/shadowk29/CUSUM>). Both analysis programs are available freely online. Nonlinear fitting results are obtained using Origin 9.1.

■ ASSOCIATED CONTENT

📄 Supporting Information

The Supporting Information is available free of charge on the ACS Publications website at DOI: 10.1021/acs.nanolett.7b03987.

Physical properties of nanofilters (Section S1); simulation setup (Section S2); analysis of passage time distributions (Section S3); size separation of dsDNA by mean passage time (Section S4); slower passage times in small control pores (Section S5); long passage time events (Section S6); folding distributions (Section S7) (PDF)

Water vapor swells the nanofilter, which is tented over an array of 200 nm high, 2 μ m diameter columns, leaving a ring cavity around each column. Newton's colors form as water vapor is breathed over top of the structure, and are eliminated as the water evaporates in room air (AVI)

Wet nanofilter stability. A wetted nanofilter (0.7 mm \times 3 mm) is exposed to repeated menisci in a microfluidic channel (AVI)

A wrinkled nanofilter is torn on meniscus. As the meniscus passes over a wrinkled nanofilter, it is torn away from the substrate and redeposited (AVI)

An illustrative simulation of an $N = 200$ (~ 3000 bp) polymer translocating through the nanofilter and eventually being captured by the sensing pore (AVI)

An animated schematic description of the fabrication and operation of the complete nanofiltered nanopore device (AVI)

■ AUTHOR INFORMATION

Corresponding Author

*E-mail: tcossa@uOttawa.ca, 613-562-5800 x6964.

ORCID

Vincent Tabard-Cossa: 0000-0003-4375-717X

Author Contributions

V.T.C. and K.B. designed the experimental study. K.B. performed nanopore experiments and wrote the first draft. K.B. and M.M. analyzed nanopore experiments. G.M. and J.L.M. developed NPN material. G.M. and K.B. developed nanofiltered pore device assembly protocols. H.W.d.H. designed the simulation study. K.K. and M.M. performed and analyzed simulations. G.M. generated schematic renders. All authors contributed to revision of the manuscript.

Funding

This work was supported in part by the Natural Sciences and Engineering Research Council of Canada (NSERC) and by the province of Ontario through their Early Researcher Award to

V.T.C., by NSF PFI-BIC no. 1237699 to J.L.M., and by NIH R21EB024120 to both V.T.C. and J.L.M.

Notes

The authors declare the following competing financial interest(s): J.L.M. declares a competing financial interest as a co-founder and equity holder of SiMPore Inc., a commercial manufacturer of NPN and silicon-based membrane materials. V.T.C. and K.B. declare a competing financial interest in the form of a patent on the nanofiltered nanopore device. All other authors declare no competing financial interests.

■ ACKNOWLEDGMENTS

The authors would like to thank James Roussie and SiMPore Inc. for generous donations of expertise and NPN membrane materials. K.B. acknowledges the financial support provided by the NSERC Vanier program for postgraduate fellowships. The authors acknowledge Tucker Burgin for this work evaluating the membrane stability of fabricated nanopore devices.

■ REFERENCES

- (1) Carson, S.; Wanunu, M. *Nanotechnology* **2015**, *26*, 1–14.
- (2) Heerema, S. J.; Dekker, C. *Nat. Nanotechnol.* **2016**, *11*, 127–136.
- (3) Dekker, C. *Nat. Nanotechnol.* **2007**, *2*, 209–215.
- (4) van Dorp, S.; Keyser, U. F.; Dekker, N. H.; Dekker, C.; Lemay, S. G. *Nat. Phys.* **2009**, *5*, 347–351.
- (5) Gershow, M.; Golovchenko, J. A. *Nat. Nanotechnol.* **2007**, *2*, 775–779.
- (6) Lu, B.; Albertorio, F.; Hoogerheide, D. P.; Golovchenko, J. A. *Biophys. J.* **2011**, *101*, 70–79.
- (7) Briggs, K.; Kwok, H.; Tabard-Cossa, V. *Small* **2014**, *10*, 2077–2086.
- (8) He, Y.; Tsutsui, M.; Fan, C.; Taniguchi, M.; Kawai, T. *ACS Nano* **2011**, *5*, 5509–5518.
- (9) Aksimentiev, A.; Heng, J. B.; Timp, G.; Schulten, K. *Biophys. J.* **2004**, *87*, 2086–2097.
- (10) Waugh, M.; Carlsen, A.; Sean, D.; Slater, G. W.; Briggs, K.; Kwok, H.; Tabard-Cossa, V. *Electrophoresis* **2015**, *36*, 1759–1767.
- (11) Squires, A. H.; Hersey, J. S.; Grinstaff, M. W.; Meller, A. *J. Am. Chem. Soc.* **2013**, *135*, 16304–16307.
- (12) Kowalczyk, S. W.; Wells, D. B.; Aksimentiev, A.; Dekker, C. *Nano Lett.* **2012**, *12*, 1038–1044.
- (13) Feng, J.; Liu, K.; Bulushev, R. D.; Khlybov, S.; Dumcenco, D.; Kis, A.; Radenovic, A. *Nat. Nanotechnol.* **2015**, *10*, 1070–1076.
- (14) Di Fiori, N.; Squires, A.; Bar, D.; Gilboa, T.; Moustakas, T. D.; Meller, A. *Nat. Nanotechnol.* **2013**, *8*, 946.
- (15) Fologea, D.; Uplinger, J.; Thomas, B.; McNabb, D. S.; Li, J. *Nano Lett.* **2005**, *5*, 1734–1737.
- (16) Larkin, J.; Henley, R.; Bell, D. C.; Cohen-Karni, T.; Rosenstein, J. K.; Wanunu, M. *ACS Nano* **2013**, *7*, 10121–10128.
- (17) Kwok, H.; Waugh, M.; Bustamante, J.; Briggs, K.; Tabard-Cossa, V. *Adv. Funct. Mater.* **2014**, *24*, 7745–7753.
- (18) Carson, S.; Wilson, J.; Aksimentiev, A.; Wanunu, M. *Biophys. J.* **2014**, *107*, 2381–2393.
- (19) Plesa, C.; van Loo, N.; Ketterer, P.; Dietz, H.; Dekker, C. *Nano Lett.* **2015**, *15*, 732–737.
- (20) Bell, N. A. W.; Keyser, U. F. *Nat. Nanotechnol.* **2016**, *11*, 1–28.
- (21) Bell, N. A. W.; Keyser, U. F. *arXiv* **2016**, 1–5.
- (22) Vollmer, S. C.; de Haan, H. W. *J. Chem. Phys.* **2016**, *145*, 154902.
- (23) Sean, D.; de Haan, H. W.; Slater, G. W. *Electrophoresis* **2015**, *36*, 682–691.
- (24) Liu, X.; Skanata, M. M.; Stein, D. *Nat. Commun.* **2015**, *6*, 6222.
- (25) Langecker, M.; Pedone, D.; Simmel, F. C.; Rant, U. *Nano Lett.* **2011**, *11*, S002–S007.
- (26) Harms, Z. D.; Mogensen, K. B.; Nunes, P. S.; Zhou, K.; Hildenbrand, B. W.; Mitra, I.; Tan, Z.; Zlotnick, A.; Kutter, J. P.; Jacobson, S. C. *Anal. Chem.* **2011**, *83*, 9573–9578.

- (27) Pedone, D.; Langecker, M.; Abstreiter, G.; Rant, U. *Nano Lett.* **2011**, *11*, 1561–1567.
- (28) Bell, N. A. W.; Chen, K.; Ghosal, S.; Ricci, M.; Keyser, U. F. *Nat. Commun.* **2017**, *8*, 380.
- (29) DesOrmeaux, J. P. S.; Winans, J. D.; Wayson, S. E.; Gaboriski, T. R.; Khire, T. S.; Striemer, C. C.; McGrath, J. L. *Nanoscale* **2014**, *6*, 10798.
- (30) Gillmer, S. R.; Fang, D. Z.; Wayson, S. E.; Winans, J. D.; Abdolrahim, N.; DesOrmeaux, J.-P. S.; Getpreecharsawas, J.; Ellis, J. D.; Fauchet, P. M.; McGrath, J. L. *Thin Solid Films* **2017**, *631*, 152–160.
- (31) Kavalenka, M. N.; Striemer, C. C.; Fang, D. Z.; Gaboriski, T. R.; McGrath, J. L.; Fauchet, P. M. *Nanotechnology* **2012**, *23*, 145706.
- (32) Kwok, H.; Briggs, K.; Tabard-Cossa, V. *PLoS One* **2014**, *9*, e92880.
- (33) Briggs, K.; Kwok, H.; Tabard-Cossa, V. *Small* **2014**, *10*, 2077–2086.
- (34) Briggs, K.; Charron, M.; Kwok, H.; Le, T.; Chahal, S.; Bustamante, J.; Waugh, M.; Tabard-Cossa, V. *Nanotechnology* **2015**, *26*, 084004.
- (35) Slater, G. W.; Holm, C.; Chubynsky, M. V.; de Haan, H. W.; Dube, A.; Grass, K.; Hickey, O. A.; Kingsburry, C.; Sean, D.; Shendruk, T. N.; Zhan, L. *Electrophoresis* **2009**, *30*, 792–818.
- (36) Mihovilovic, M.; Hagerty, N.; Stein, D. *Phys. Rev. Lett.* **2013**, *110*, 1–5.
- (37) Carlsen, A. T.; Zahid, O. K.; Ruzicka, J.; Taylor, E. W.; Hall, A. R. *ACS Nano* **2014**, *8*, 4754–4760.
- (38) Storm, A. J.; Chen, J. H.; Zandbergen, H. W.; Dekker, C. *Phys. Rev. E* **2005**, *71*, 51903.
- (39) Storm, A. J.; Storm, C.; Chen, J.; Zandbergen, H. *Nano Lett.* **2005**, *5*, 1–5.
- (40) De Haan, H. W.; Sean, D.; Slater, G. W. *Phys. Rev. E* **2015**, *91*, 1–10.
- (41) Ikonen, T.; Bhattacharya, A.; Ala-Nissila, T.; Sung, W. *Phys. Rev. E* **2012**, *85*, 1–7.
- (42) Teraoka, I. *Polymer Solutions: An Introduction to Physical Properties*; John Wiley & Sons, Inc, 2002.
- (43) Farahpour, F.; Maleknejad, A.; Varnik, F.; Eftehadi, M. R. *Soft Matter* **2013**, *9*, 2750.
- (44) Rowghanian, P.; Grosberg, A. Y. *Phys. Rev. E* **2013**, *87*, 1–8.
- (45) Morin, T. J.; Shropshire, T.; Liu, X.; Briggs, K.; Huynh, C.; Tabard-Cossa, V.; Wang, H.; Dunbar, W. B. *PLoS One* **2016**, *11*, e0154426.
- (46) Singer, A.; Wanunu, M.; Morrison, W.; Kuhn, H.; Frank-kamenetskii, M.; Meller, A. *Nano Lett.* **2010**, *10*, 738–742.
- (47) Atas, E.; Singer, A.; Meller, A. *Electrophoresis* **2012**, *33*, 3437–3447.
- (48) Plesa, C.; Ruitenbergh, J. W.; Witteveen, M. J.; Dekker, C. *Nano Lett.* **2015**, *15*, 3153–3158.
- (49) van den Hout, M.; Hall, A. R.; Wu, M. Y.; Zandbergen, H. W.; Dekker, C.; Dekker, N. H. *Nanotechnology* **2010**, *21*, 115304.
- (50) Rollings, R.; Graef, E.; Walsh, N.; Nandivada, S.; Benamara, M.; Li, J. *Nanotechnology* **2015**, *26*, 997–1003.
- (51) Balijepalli, A.; Ettetdgui, J.; Cornio, A. T.; Robertson, J. W. F.; Cheung, K. P.; Kasianowicz, J. J.; Vaz, C. *ACS Nano* **2014**, *8*, 1547–1553.
- (52) Forstater, J. H.; Briggs, K.; Robertson, J. W. F.; Ettetdgui, J.; Marie-Rose, O.; Vaz, C.; Kasianowicz, J. J.; Tabard-Cossa, V.; Balijepalli, A. *Anal. Chem.* **2016**, *88*, 11900–11907.
- (53) Raillon, C.; Granjon, P.; Graf, M.; Steinbock, L. J.; Radenovic, A. *Nanoscale* **2012**, *4*, 4916–4924.